



Catalytic cleavage of the β -O-4 aryl ether bonds of lignin model compounds by Ru/C catalyst

Md Anwar Hossain^{a,1}, Thanh Khoa Phung^{a,b,c,1}, Mohammad Shahinur Rahaman^a, Sarttrawut Tulaphol^d, Jacek B. Jasinski^{a,b}, Noppadon Sathitsuksanoh^{a,*}

^a Department of Chemical Engineering, University of Louisville, Louisville, KY, 40292, United States

^b Conn Center for Renewable Energy Research, University of Louisville, Louisville, KY, 40292, United States

^c International University, Vietnam National University – HCMC, Quarter 6, Linh Trung Ward, Thu Duc District, Ho Chi Minh City, Viet Nam

^d Department of Chemistry, King Mongkut's University of Technology Thonburi, Bangkok, 10140, Thailand

ARTICLE INFO

Keywords:

Lignin
Ruthenium
Self-hydrogen
Hydrogenolysis
Hydrogen transfer

ABSTRACT

Lignin is a potential renewable feedstock for aromatic compounds. Lignin glues cellulose and hemicellulose together in a rigid structure that protects plants from weather, insects, and disease. This rigidity also poses a barrier to cleavage of lignin into aromatic compounds. Typically, lignin is depolymerized by metal-catalyzed hydrogenolysis of its β -O-4 aryl ether (C_{β} -O) bonds; this process requires high H_2 pressure. Here, we show that the abundant aliphatic hydroxyl groups (C_{α} -OH) in lignin structure, can serve as the hydrogen source in Ru-catalyzed hydrogenolysis of the C_{β} -O bonds. We pretreated the Ru/C catalyst under reducing and oxidizing conditions to generate various Ru/RuO₂ ratios. Then we investigated the effects of Ru and RuO₂ on hydrogenolysis of the C_{β} -O bonds of lignin model compounds. We used X-ray diffraction (XRD) and H_2 Temperature-programmed reduction (TPR) to determine changes of grain size and Ru content of the Ru/C catalysts, respectively. Our results revealed that Ru/C catalyzed hydrogenolysis of β -O-4 aryl ether bonds with internal hydrogen (self-hydrogen) as a hydrogen source. The elimination of external H_2 in lignin hydrogenolysis is an efficient approach for lignin conversion to valuable aromatic chemicals.

1. Introduction

Lignin is a by-product of paper and pulp manufacturing and biorefineries [1–3]. Lignin has aromatic backbones, making it an ideal renewable feedstock of aromatic compounds for a range of applications, including automotive brakes, wood panel products, surfactants, phenolic resins, phenolic foams, bio-dispersants polyurethane foams, and epoxy resins [4–12]. Despite this great potential for high-value exploitation, only ~5% of lignin by-products have been used in mostly low-value commercial applications, such as the production of low-grade fuels for heat and power and as concrete additives [4,8]. One reason for this restricted usage is that the complex chemical structure of lignin makes it difficult to release its aromatic monomers.

Typically, lignin is composed of three major phenolic monomers (monolignols): (1) *p*-coumaryl alcohol, (2) coniferyl alcohol, and (3) sinapyl alcohol. These monolignols are polymerized into lignin in the form of phenylpropanoid units (a phenyl (C_6) + a propane (C_3)), *p*-hydroxyphenyl (H), guaiacyl (G), and syringyl (S) units. These

phenylpropanoid units are joined to form C_{β} -O (β -O-4 aryl ether) and C-C (β -5 and β - β) bonds (Fig. 1 (adapted from Ref. [13])). Lignin contains ~50–65% β -O-4 aryl ether bonds and abundant aliphatic and aromatic hydroxyl groups [14]. These linkages and functional groups make lignin a stiff and rigid structure, giving plants strength and protecting them from external disturbances such as insects, disease, and weather. This rigid structure of lignin is another reason why it is difficult to break lignin into aromatic monomers.

To release renewable aromatic monomers, investigators have used hydrogenolysis by metal catalysts, such as Ru/C, Ni/C, Pd/C, Pd/Al₂O₃, CuMgO_x, NiRu, and CuCr₂O₄/CuO, to break the abundant C_{β} -O bonds of lignin [15–26]. Typically, a high H_2 pressure (≥ 10 bar) is required for hydrogenolysis [22,27,28]; however, the high H_2 pressure causes undesired side reactions of over-hydrogenating the aromatic rings, cracking, and coke formation [27]. Moreover, the hydrogen sources are not naturally available and renewable, making H_2 -mediated hydrogenolysis uneconomic on a large scale [29,30]. To minimize the effect of side reactions, the industry requires hydrogen-lean or hydrogen-free

* Corresponding author.

E-mail address: N.sathitsuksanoh@louisville.edu (N. Sathitsuksanoh).

¹ These authors contributed equally to this work.

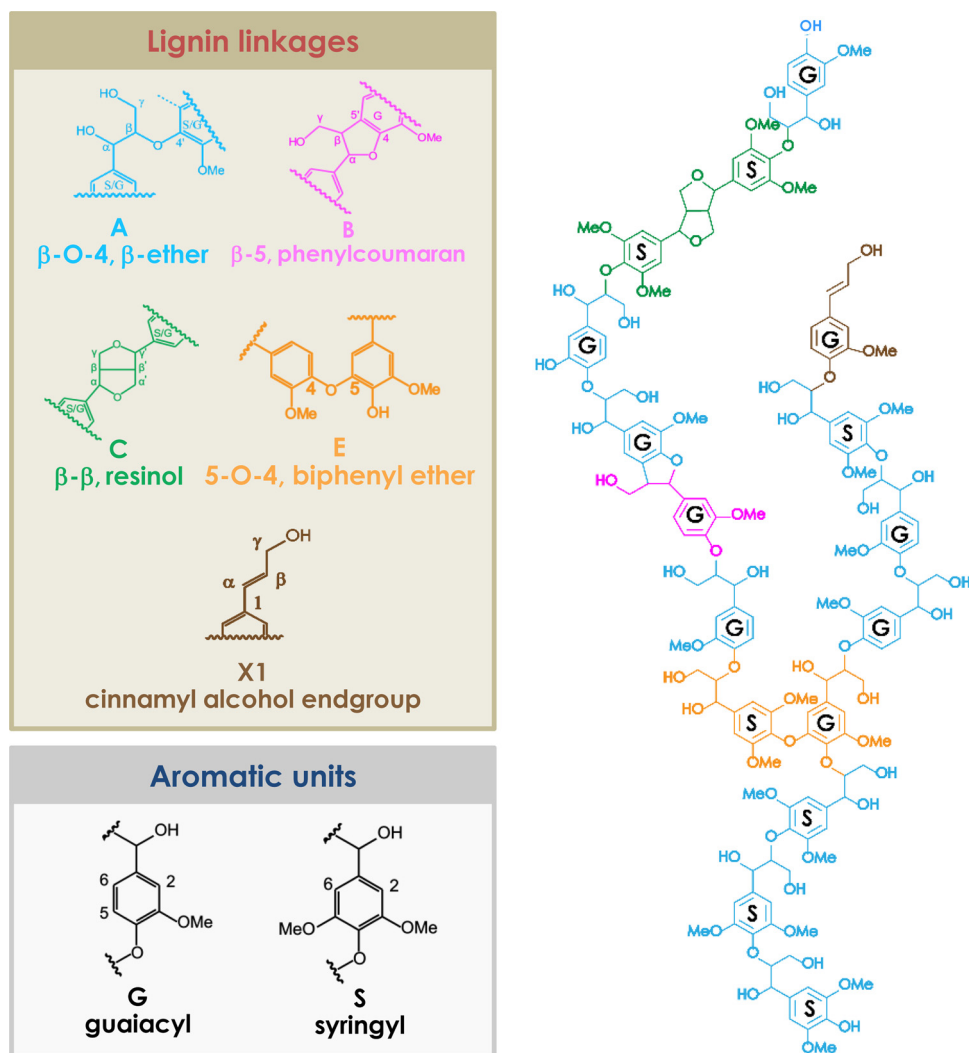


Fig. 1. An example of a truncated (poplar) lignin structure. This lignin model depicts β -O-4 aryl ether bonds as the abundant linkages.

catalytic systems.

Oxophilic metals, such as ruthenium (Ru), have partially filled d-bands. The oxophilicity of Ru enables strong interaction with oxygen atoms in the adsorbates, resulting in the direct cleavage of C–O bonds [31–33]. Previous studies have shown that reducible RuO₂ catalysts have Lewis acid sites that facilitate the hydrodeoxygenation of furanics in the liquid phase [34,35]. Supported Ru catalysts have been applied to the hydrogenolysis of lignin and its model compounds [36,37], the effect of Ru and RuO₂ on the hydrogenolysis and hydrodeoxygenation of lignin is not well understood. The partial oxidation of Ru to RuRuO₂ creates a bifunctional catalyst containing: (1) Ru metal sites, catalyzing hydrogenolysis/hydrogenation; and (2) RuO₂ Lewis acid sites, facilitating hydrogenolysis [34]. We hypothesized that the aliphatic –OH groups (C_α–OH) of lignin could serve as internal hydrogen donors; the released hydrogen would break lignin's C_β–O bonds without further aromatic ring saturation. We further expected that this hydrogenolysis reaction would occur with a Ru/C catalyst having an optimal Ru/RuO₂ composition.

To test these conjectures, we synthesized Ru/C catalysts with various ratios of Ru/RuO₂ and assessed their activities in hydrogenolysis of the C_β–O bond in two lignin model compounds: 2-phenoxy-1-phenylethanol and 2-phenyl ethyl phenyl ether. The aliphatic C_α–OH group of 2-phenoxy-1-phenylethanol enabled the hydrogenolysis of the C_β–O bonds in the absence of H₂. An increase in Ru content enhanced hydrogenolysis activity. The elimination of the H₂ requirement in lignin

hydrogenolysis provides a simple yet efficient approach for lignin conversion to aromatic chemicals.

2. Experimental

2.1. Materials

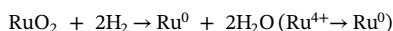
All reagents were used as received. Their manufacturers, purity, and CAS numbers are shown in Table S1.

2.2. Catalysts pretreatment and characterization

To tailor the catalyst composition, the commercial Ru/C catalyst (parental Ru/C) was treated in various conditions before catalytic testing. For reduction, the fresh Ru/C catalyst was reduced in H₂ flow of 40 cc/min at 250 °C for 3 h, followed by the 12 h passivation in air, to form the Ru/C-Red catalyst. For oxidation, the fresh Ru/C catalyst was oxidized in pure O₂ flow of 40 cc/min at 200 °C for 3 h to create the Ru/C-O x catalyst. The commercial Ru/C and commercial pre-reduced Ru/C catalysts were also used as references. Descriptions of these Ru/C catalysts and their pretreatment conditions are summarized in Table S2.

X-ray diffraction (XRD) was performed with a Bruker D8 Discover diffractometer (Billerica, MA, USA) using CuK α radiation in the 2 θ range from 20° to 60° with 1 s/step (0.02 increment). H₂ Temperature-

Programmed Reduction (H_2 -TPR) experiments were performed with a Micromeritics ChemiSorb 2720 equipped with a thermal conductivity detector (TCD) (Norcross, GA, USA). About 20–40 mg of sample was pretreated at 250 °C for 1 h under He flow to remove adsorbed water. Then, the sample was cooled to room temperature under He flow. TPR profiles were recorded by heating the samples from room temperature to 800 °C at a heating rate of 10 °C/min in the 10.01% H_2/Ar at a flow rate of 40 cc/min. The RuO_2 content in the Ru/C catalysts was calculated by the following reaction:



H_2 consumption and mole of metallic Ru and RuO_2 were calculated using the known H_2 (vol.%) as a calibrant as follows:

$$H_2 \text{ consumption (mol } H_2/\text{g total Ru)} = \frac{\sum \text{Area}_{\text{outlet peaks}}}{\text{Area}_{\text{calibrant}}} \times \frac{\text{mole}_{\text{calibrant}}(\text{mol})}{\text{mass}_{\text{catalyst}}(\text{g})} \times \frac{1}{\text{Ru loading (wt.%)}}$$

$$\text{mole}_{RuO_2}(\text{mol}) = \text{mole}_{O_2} = \frac{1}{2} \text{mole}_{H_2 \text{ consumption}}$$

$$\text{mole}_{\text{metallic Ru}}(\text{mol}) = \text{mole}_{\text{total Ru}} - \text{mole}_{RuO_2}$$

$$RuO_2 \text{ in total Ru (mol.}\%) = \frac{\text{mole}_{RuO_2}}{\text{mole}_{Ru} + \text{mole}_{RuO_2}} \times 100$$

Energy Dispersive X-ray Spectroscopy (EDS) was conducted on the spent Ru/C catalyst to assess the change in the Ru content after the reaction. EDS was performed on the Thermo Scientific™ FEI Nova600 FEG Scanning Electron Microscope (SEM) equipped with EDS (Hillsboro, OR, USA).

2.3. Hydrogenolysis of lignin model compounds

All reactions were performed in a 25 mL autoclave reactor (Parr Instrument, Moline, IL, USA). The reactant concentrations were 1 wt.% of 2-phenoxy-1-phenylethanol or 2-phenyl ethyl phenyl ether in ethanol. The catalyst loading was 20 wt.% (~18.9 mg catalyst) with respect to the reactant (94.68 mg reactant in 12 mL ethanol solution). Prior to the reaction, the reactor was purged three times with N_2 to remove O_2 . The reactor was then pressurized to 8 bar under N_2 at room temperature (for consistency). The hydrogenolysis reaction was performed at 280 °C for 4 h with a stirring rate of 500 rpm. The reaction was stopped by quenching in a cold water bath. The reaction sample was centrifuged to remove any residual solids, then diluted with ethanol prior to the product analysis. Dodecane was used as an internal standard.

The reactants and products were identified and quantified by the Agilent 7890B GC (Agilent Technologies, Santa Clara, CA, USA) equipped with Mass spectrometry (MS) and Flame Ionization Detectors (FID). An HP-5MS column (30mx0.25mmx0.25 μ m, Agilent Technologies, Santa Clara, CA, USA) was used for product separation with the following temperature program: injection temperature 275 °C and FID detector temperature 300 °C; split ratio 1:50. The temperature program started at 45 °C and increased at 10 °C/min to 250 °C, then held for 20 min. Reactant conversion, product selectivity, and specific activity were calculated using the pre-determined response factors with dodecane as an internal standard. The calculations are as follows:

$$\text{Conversion (\%)} = \frac{\text{mole of reactant reacted}}{\text{initial mole of reactant}} \times 100\%$$

$$\text{Selectivity (\%)} = \frac{\text{mole of product generated}}{\text{mole of feed reacted}} \times 100\%$$

$$\text{Specific activity (mmol/(g}_{Ru} \cdot h)) = \frac{\text{mole of feed reacted}}{\text{weight of Ru} \times \text{time}}$$

2.4. Catalyst stability evaluation

The catalyst stability was examined by conducting catalyst recycling experiments for four times. After the reaction, the spent catalyst was recovered by filtration and reused without washing/drying in the next experiment. The reactants and products from each recycle run were quantified by GC-MS/FID. The Ru content of the spent catalyst from each recycle run was analyzed by H_2 -TPR. In separate experiments, the spent catalyst was sampled with the reaction products after each recycle run into the U-shaped reactors directly for H_2 -TPR to minimize the catalyst oxidation in air.

3. Results and discussion

To examine the effect of metallic Ru and RuO_2 on the hydrogenolysis of the C_{β} -O bonds, we varied the amount of Ru and RuO_2 by treating the parental Ru/C in various conditions (Table S2). The commercial pre-reduced Ru/C served as the control. We used H_2 -TPR and XRD to determine the amount of RuO_2 in these four catalysts and identify their phases, respectively. We correlated changes in Ru content with the hydrogenolysis activities of the catalysts toward the C_{β} -O bonds of the lignin model compounds.

3.1. Catalysts pretreatment and their reducibility

The relative Ru and RuO_2 content in Ru/C catalyst play an important role in hydrogenolysis of the C_{β} -O bonds. We first used the H_2 -TPR technique to determine the amount of Ru and RuO_2 in the four catalysts. Using H_2 as a stoichiometric reductant, we found that, as the catalyst temperature increased from 50 to 350 °C, the reduction profiles of Ru/C catalysts showed two major reduction peaks. The first reduction peak appeared at < 100 °C and the second reduction peak occurred at > 100 °C (Fig. 2). The presence of two reduction peaks suggested that ruthenium took different oxidation states while reducing from Ru^{4+} (RuO_2) to Ru^0 (metallic Ru). The H_2 -TPR profile of the pre-reduced Ru/C showed a small reduction peak at 74 °C. This reduction peak was observed previously in Ru/CeO_2 and Ru/C catalysts [38]. The commercial Ru/C catalyst (parent) had two observable reduction peaks

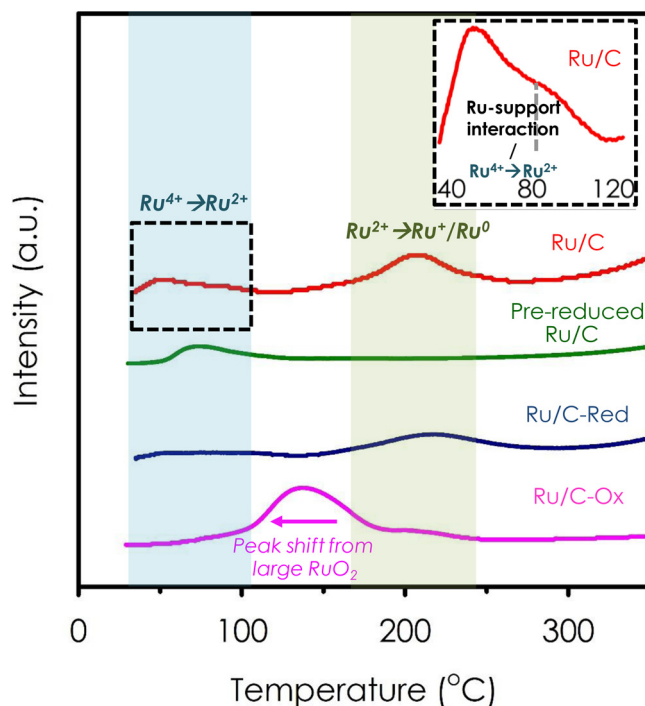


Fig. 2. H_2 -TPR profiles of Ru/C catalyst from different pretreatment conditions.

at $< 100^\circ\text{C}$ and $> 200^\circ\text{C}$ with a shoulder peak at 246°C . The first reduction peak at low temperature appeared to be broad doublets. Other investigators have observed doublets with Ru supported on Al_2O_3 , ZrO_2 , CeO_2 , and carbon [32,38,39]. Doublets are hypothesized to form because of (1) the strong interaction between Ru species and the support [38,40], and (2) the reduction of Ru^{4+} to Ru^{2+} , suggesting the formation of easily reducible surface species. The second reduction peak ($> 200^\circ\text{C}$) could be assigned to the reduction of Ru^{2+} to Ru^+ or the reduction of Ru^{2+} to Ru^0 (metallic Ru) [41–46]. After reducing the parental Ru/C in H_2 , the second reduction peak at 205°C and the shoulder peak at 246°C disappeared (Figure S1) and the H_2 -TPR profile became similar to that of pre-reduced Ru/C. This result suggested that this H_2 -TPR condition was sufficient to completely reduce the Ru^{4+} to Ru^0 . Then, we allowed this catalyst to passivate in the air for 12 h to generate partial RuO_2 phase. We used the term Ru/C-Red to represent this sample. The Ru/C-Red had a similar H_2 -TPR profile to that of Ru/C. However, its first reduction peak was rather broad and the second reduction peak was shifted to a higher temperature (217°C) compared with that of the parental Ru/C (205°C). Next, we oxidized the parental Ru/C using O_2 flow at 200°C for 3 h to obtain the Ru/C-O x sample. We observed a shift of the second reduction peak from 205°C to 135°C , indicating that there were structural changes in RuO_2 from oxidation. The large reduction peak at 135°C on the Ru/C-O x resulted from the formation of larger RuO_2 particle sizes, decreasing the interaction between supports and RuO_2 [47–51]. We also used these H_2 -TPR profiles to determine the Ru and RuO_2 content in all catalysts.

The Ru content in the Ru/C catalysts, calculated based on the H_2 consumption, was in the following order: pre-reduced Ru/C (95.3%) $>$ Ru/C-Red (85.5%) $>$ Ru/C (82.0%) $>$ Ru/C-O x (74.7%) (Table S3). The parental Ru/C catalyst had $\sim 82\%$ Ru (metallic) and $\sim 18\%$ RuO_2 . Ru/C-Red, reduced Ru/C catalyst by H_2 and passivated in the air to generate RuO_2 , had a 22% decrease in RuO_2 content. After oxidizing the parental Ru/C, the RuO_2 content of the Ru/C-O x increased $\sim 28\%$ compared to that of parental Ru/C. For Ru/C-O x, the carbon support was oxidized during the pretreatment, causing a relative increase in Ru content per total gram of Ru/C-O x. We used thermogravimetric analysis of the Ru/C catalysts, phase identification by XRD spectra, and an estimated amount of RuO_2 and Ru content by H_2 -TPR to determine the mass percentage of Ru, RuO_2 , and C (Table S4). These results indicated that after oxidation, the Ru/C-O x lost carbon support by $\sim 22\text{ wt.}\%$. These Ru/C catalysts were used in the hydrogenolysis of the lignin model compounds.

H_2 -TPR results confirmed the reducibility of the Ru/C catalysts. They demonstrated that we could tune the oxidation state of Ru/C under various pretreatment conditions [52]. Our results also illustrated that ruthenium was easily passivated, as shown in the formation of RuO_2 under the ambient condition. The use of commercial Ru/C catalyst needs to be with cautions because it can be passivated, affecting the Ru and RuO_2 contents. The catalyst pretreatment conditions affected the grain size and dispersion/agglomeration of Ru catalysts on supports. For example, the shift of the reduction peak to the lower reduction temperature of the Ru/C-O x (compared to that of parental Ru/C) suggested an increase in the grain size of the RuO_2 . The change in grain size of catalyst also affects its catalytic activity [53]. To identify changes in Ru and RuO_2 phases and grain size of catalysts, we applied the XRD technique on all catalysts.

3.2. Identification of Ru and RuO_2 phases and determination of catalyst grain sizes

XRD spectra of Ru/C catalysts revealed the Ru and RuO_2 phases and their degrees of dispersion on the carbon support (Fig. 3). The parental Ru/C and pre-reduced Ru/C catalysts had broad XRD spectra, suggesting that (1) the metallic Ru and RuO_2 were highly dispersed on the carbon, and (2) their grain sizes were small [26]. After the reduction in H_2 and passivation, the Ru/C-Red illustrated three XRD peaks,

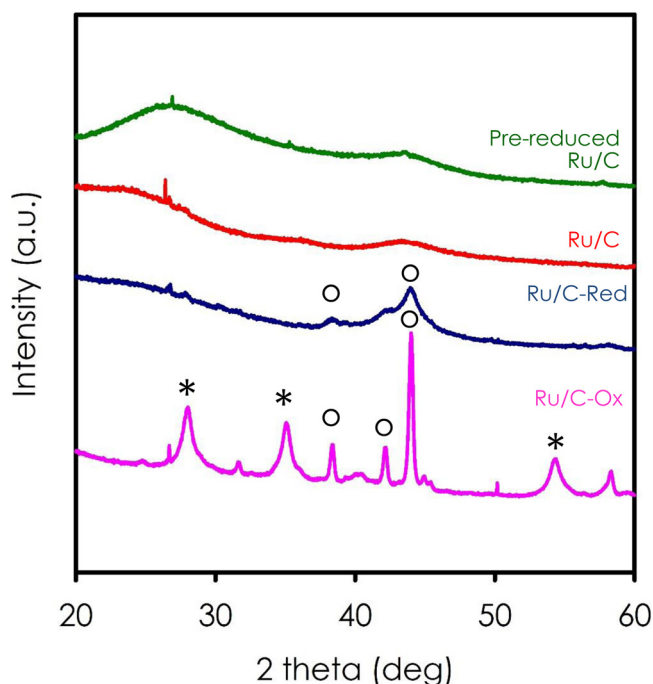


Fig. 3. XRD patterns of Ru/C catalyst from different pretreatment conditions. Note: metallic Ru (○) and RuO_2 (*).

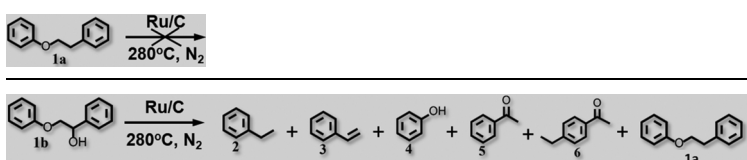
associated with the presence of metallic Ru at 2θ of $\sim 39^\circ$ for Ru(100), 42° for Ru(002), and 44° for Ru(101) [46,54]. The crystallite sizes of the Ru catalysts were calculated from the Debye-Scherrer equation and the broadening of the main peaks [55]. The mean crystallite size was $\sim 4.4\text{ nm}$ for Ru(100) and Ru(101). The peak Ru(002) had low intensity, and we did not calculate its crystallite size. In the case of Ru/C-O x, we observed sharp XRD peaks associated with the presence of Ru and RuO_2 . The three XRD diffraction peaks of Ru (100), (002), and (101) became more pronounced compared with the diffraction peaks from the Ru/C post-reduction. This increase in peak intensity resulted from (1) the lower content of the carbon support due to the oxidation of carbon and (2) the sintering of the Ru, which formed larger Ru aggregates. Our calculation showed that the crystallite size of the Ru was $\sim 19\text{--}25\text{ nm}$. Three XRD peaks of RuO_2 emerged, corresponding to $\text{RuO}_2(110)$, $\text{RuO}_2(101)$, and $\text{RuO}_2(211)$ at 2θ of 28, 35, and 54° respectively [44–46]. We attributed the emergence of these RuO_2 peaks to (1) the oxidation of the metallic Ru, forming RuO_2 and/or (2) the sintering of the RuO_2 particles into larger RuO_2 particles. The crystallite sizes of RuO_2 were determined to be $\sim 6\text{--}10\text{ nm}$. The formation of the larger RuO_2 particles observed by XRD corroborated the shift of the reduction temperature to lower temperature in the H_2 -TPR profile.

3.3. Catalytic activity of parental Ru/C catalyst in hydrogenolysis of the β -O-4 aryl ether bond

We tuned the Ru/C catalyst's oxidation states under various oxidation and reduction conditions, generating four catalysts, Ru/C, pre-reduced Ru/C, Ru/C-Red and Ru/C-O x. Then we characterized these catalysts by H_2 -TPR to determine the Ru content and probed for their hydrogenolysis activity on lignin model compounds. To assess the activity of the C_α -hydroxyl ($\text{C}_\alpha\text{-OH}$) group on the hydrogenolysis of the $\text{C}_\beta\text{-O}$ bond, we first tested the parental Ru/C on 2-phenethyl phenyl ether (1a) and 2-phenoxy-1-phenylethanol (1b) under N_2 . The parental Ru/C was not active for hydrogenolysis of 2-phenethyl phenyl ether (1a), whereas it promoted 52.5% conversion on 2-phenoxy-1-phenylethanol (1b) (Table 1). Ethylbenzene (2) and phenol (4) were major reaction products, confirming the occurrence of the hydrogenolysis

Table 1

Conversion and product selectivity from hydrogenolysis of 2-phenethyl phenyl ether (1a) and 2-phenoxy-1-phenylethanol (1b) over Ru/C catalyst.



Entry	Feed	Conversion (%)	Selectivity (%)					
			2	3	4	5	6	1a
1	1a	–	–	–	–	–	–	–
2	1b	52.5	25.4	6.8	34.6	8.2	3.7	20.1
3	1b*	52.7	13.2	7.4	33.6	21.9	–	13.6

Reaction condition: 280 °C, 4 h, 8 bar N₂, 1 wt.% reactant/ethanol, 20 wt.% catalyst loading. * 1,4-dioxane was used as a solvent.

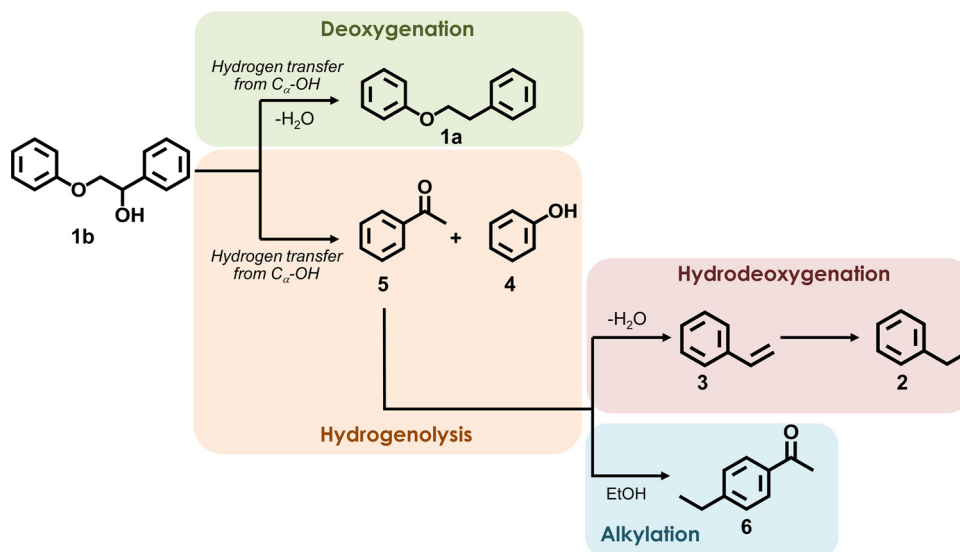
reaction. Typically, hydrogenolysis of the C_β-O bond requires high H₂ pressure and metal catalysts, including NiMo sulfide, Ni, and Pd [22,27,28,56]. However, our results showed that the –OH group at the C_α position (C_α-OH) enabled cleavage of the C_β-O bond by Ru/C at 280 °C in the absence of H₂.

Zhang et al. observed similar products for hydrogenolysis of 2-phenoxy-1-phenylethanol on NiMo sulfide catalysts, but H₂ and alcohol were needed [57]. Based on our identified reaction products (Table 1), we proposed a reaction pathway (Fig. 4) wherein Ru/C catalyzed the hydrogenolysis of C_β-O bond of 2-phenoxy-1-phenylethanol (1b) by activation of C_α-OH. The activation of C_α-OH resulted in hydrogen transfer and the hydrogenolysis of C_β-O bond and yielded phenol (4) and phenylethanone (5). If the Ru/C catalyst only catalyzed hydrogenolysis of the C_β-O bond of 2-phenoxy-1-phenylethanol (1b), we could only observe phenol (4) and phenylethanone (5). In our case, the presence of 2-phenethyl phenyl ether (1a), ethylbenzene (2), styrene (3), and *p*-ethylacetophenone (6) indicated that Ru also catalyzed side reactions. The presence of styrene (3) and ethylbenzene (2) suggested that 1-phenylethanone (5) underwent hydrodeoxygenation to form styrene as an intermediate. The styrene was then hydrogenated to ethylbenzene.

The formation of *p*-ethylacetophenone (6) occurred by the alkylation of phenylethanone (5) and ethanol. We did not observe this product when the reaction was run in dioxane. Moreover, in dioxane as a solvent, the selectivity toward *p*-ethylacetophenone (6) was low (< 4%). Ru/C also catalytically cleaved C_α-OH of 2-phenoxy-1-

phenylethanol, forming 2-phenethyl phenyl ether (1a) by the undesired deoxygenation pathway [58]. Cao et al. used PdCl₂, Pd/C, and Ru/C under 70 bar CO₂ and found a high yield of 2-phenethyl phenyl ether (1a) [59]. In that study, the formation of 2-phenethyl phenyl ether (1a) resulted from the formation of the better leaving group, –OH₂⁺, derived from the hydroxyl group at the C_α-OH position with the second hydrogen derived from ethanol [59].

Although our result suggested that Ru/C activated the C_α-OH to release its hydrogen for hydrogenolysis of the C_β-O bond in an ethanol solvent, we could not rule out the possibility that hydrogen was derived from ethanol. Ethanol is a polar protic solvent, known to donate hydrogen under the reaction condition we employed. Thus, to decouple the contribution of hydrogen from C_α-OH and ethanol, we ran a similar experiment using a non-hydrogen donor solvent, the aprotic polar solvent 1,4-dioxane. Interestingly, we obtained 52.7% conversion of 2-phenoxy-1-phenylethanol (1b), similar to the yield in the ethanol solvent (Entry 3, Table 1). However, using dioxane as a solvent, we found a lower selectivity toward aromatic hydrocarbon products (Σ(2,3) = 20.6%) compared with selectivity in ethanol (32.2%). A previous study on hydrogenolysis of 2-phenethyl phenyl ether (1a) on Pd/C showed a 30% yield of ethylbenzene (2) in isopropanol, but ethylbenzene is not observed in dioxane and toluene [60]. These results demonstrated that Ru activated C_α-OH, releasing hydrogen to form “hydrogen pool” for hydrogenation to cleave C_β-O bond [60]. Moreover, ethanol promoted the hydrodeoxygenation reaction as shown by a higher selectivity toward aromatic hydrocarbon products compared

**Fig. 4.** The proposed reaction pathway of hydrogenolysis of 2-phenoxy-1-phenylethanol over Ru/C catalyst with C_α-OH as the hydrogen source.

with selectivity in dioxane. In addition, ethanol can be obtained from renewable resources. For these reasons, we used ethanol in the remaining studies. Next, we wanted to compare the effect of Ru content in the Ru/C catalyst in hydrogenolysis of C_β-O bond. We tuned the Ru content by applying various pretreatment conditions.

3.4. Catalytic activity of Ru and RuO₂ catalysts in hydrogenolysis of the β-O-4 aryl ether bond

To assess the effects of Ru and RuO₂ in hydrogenolysis of the C_β-O bond, we evaluated Ru/C catalysts under various pretreatment conditions to obtain various Ru content (Table S5). For each Ru/C catalyst, we calculated the catalytic activity for reactant conversion per (total) gram of Ru per unit time. The reaction using the pre-reduced Ru/C had the highest hydrogenolysis activity of 112 mmol reactant/g_{Ru}*h, whereas the Ru/C-O x had the lowest hydrogenolysis activity of 4 mmol reactant/g_{Ru}*h. One reason for this difference is that the Ru/C-O x had the highest RuO₂ content (25%) and large crystallite sizes of Ru and RuO₂ (~19–25 nm for Ru and ~6–10 nm for RuO₂) from aggregation and/or sintering of the small Ru and RuO₂ particles. The large Ru crystallite size lowered the surface of the active sites, resulting in lower catalytic activity [53]. Moreover, RuO₂ has a weak oxygen surface bonding to bridge oxygen atoms on the RuO₂ surface [61]. Conversely, metallic Ru has a strong adsorption interaction with oxygen and –OH group [62–64], which promotes the hydrodeoxygenation of 2-phenethyl phenyl ether (1a) and ethylbenzene (2). The increasing trend of the catalytic activity with increasing metallic Ru suggested that the metallic Ru was the active phase for the hydrogenolysis of C_β-O bonds. Moreover, metallic Ru was the active site that activated C_α-OH, releasing this “self-hydrogen” from 2-phenoxy-1-phenylethanol (1b).

The surface of RuO₂ on the Ru/C catalyst exists upon oxidation of Ru when exposed to air during storage/handling. Our H₂-TPR results also showed that Ru was passivated under the ambient condition, changing the Ru and RuO₂ contents and affecting catalytic activity. The use of alcohol as a solvent is beneficial because alcohol can reduce the RuO₂ in-situ, maintaining the catalyst in the active form and enhancing the catalytic activity over time [65]. We hypothesized that, during the reaction, RuO₂ would be reduced in-situ when ethanol was the solvent [66,67], enhancing the catalytic activity. To test this hypothesis, we performed the hydrogenolysis of the 2-phenethyl phenyl ethanol (1b) in ethanol over 12 h. We determined the Ru content of the spent catalyst by sampling the spent catalyst with the reaction products after each reaction into the U-shaped reactors directly for H₂-TPR. By doing so, we minimized the catalyst oxidation in air. We observed an increase in reactant conversion over time and reached 99.7% after 12 h (Table S6). Moreover, the Ru content of the spent catalyst increased as a function of time and reached 3.5% at 12 h (Figure S2). The selectivity toward aromatic product yields (Σ(2,3)) remained ~31–35% regardless of reaction time. This increase in reactant conversion was correlated with an increase in metallic Ru from the in-situ RuO₂ reduction in ethanol.

3.5. Catalyst stability and its recyclability

Metallic Ru was an active phase for hydrogenolysis of 1b and the Ru/C catalysts were reduced in-situ in the presence of ethanol. To assess the stability of the Ru/C catalyst, we recycled our catalyst four times and determined the reactant conversion and product selectivity. We used H₂-TPR to determine changes in the Ru content of the spent Ru/C catalysts after each recycle. We observed a slight increase in metallic Ru content after recycles (Figure S3). The reactant conversion increased in the second recycle from

52.5% (fresh Ru/C) to 73.1% (after second recycle) (Table S7) and progressively decreased to 55.5% after four recycles. With these results, we hypothesized that the catalyst deactivated because of the Ru leaching out of the carbon support into the solution. Thus, we performed an elemental analysis of the spent catalyst by EDS. Our EDS

results showed ~50 wt.% decrease in Ru content in the spent catalyst after four recycles. These results suggested that the Ru was not stable in ethanol under the investigated condition and leached out in the solution. Previous studies have shown a similar leaching behavior of Ru into the reaction solution [68–70]. The stability of supported Ru depends on many factors, such as Ru precursors, types of supports, reaction solvents, and interactions between catalyst with reactants/intermediates/products [71]. Further investigation is needed to identify the root cause of Ru leaching and to improve the stability of the supported Ru for hydrogenolysis of lignin model compounds.

4. Conclusions

Lignin is a potential renewable aromatic feedstock. Rigidity and cross-linked lignin polymers make lignin difficult to be cleaved, releasing monoaromatic compounds. Lignin consists of ~50–65% β-O-4 aryl ether (C_β-O) bonds and abundant aliphatic and aromatic hydroxyl groups. We have demonstrated that the Ru catalyst catalyzed the hydrogenolysis of C_β-O bonds of a lignin model compound using the internal hydrogen source from C_α-OH. These results provide an alternative and efficient strategy for lignin conversion without a requirement for external, high-pressure H₂. We pretreated Ru catalysts in various conditions and identified the metallic Ru as the active phase for hydrogenolysis of C_β-O bonds. X-ray diffraction (XRD) and H₂ Temperature-programmed reduction (TPR) measurements supported that the Ru was the active site for hydrogenolysis of C_β-O bonds. The use of alcohol as a reaction solvent enabled the in-situ reduction of RuO₂ from Ru/C, increasing catalytic activity over time. These results have potential application in lignin conversion to aromatic chemicals from pulp and paper manufacturing and from biorefineries.

Acknowledgment

This work was supported in part by the National Science Foundation under Cooperative Agreement No. 1355438. This work was performed in part at the Conn Center for Renewable Energy Research at the University of Louisville, which belongs to the National Science Foundation NNCI KY Manufacturing and Nano Integration Node, supported by ECCS-1542174. The authors thank Dr. Howard Fried for his comments and suggestions on the manuscript.

Appendix A. Supplementary data

Supplementary material related to this article can be found, in the online version, at doi:<https://doi.org/10.1016/j.apcata.2019.05.034>.

References

- [1] A. Duval, F. Vilaplana, C. Crestini, M. Lawoko, *Holzforchung* 70 (2015) 11–20.
- [2] J. Hu, Q. Zhang, D.-J. Lee, *Bioresour. Technol.* 247 (2018) 1181–1183.
- [3] S. Sathawong, W. Sridach, K. Techato, *J. Environ. Chem. Eng.* 6 (2018) 5879–5888.
- [4] L. Hu, H. Pan, Y. Zhou, M. Zhang, *Bioresour.* 6 (2011) 3515–3525.
- [5] S.-H. Lee, Y. Teramoto, N. Shiraiishi, *J. Appl. Polym. Sci.* 84 (2002) 468–472.
- [6] J.H. Lora, W.G. Glasser, *J. Polym. Environ.* 10 (2002) 39–48.
- [7] R. Gosselink, E. De Jong, B. Guran, A. Abächerli, *Ind. Crops Prod.* 20 (2004) 121–129.
- [8] C. Li, X. Zhao, A. Wang, G.W. Huber, T. Zhang, *Chem. Rev.* 115 (2015) 11559–11624.
- [9] Y. Zheng, D. Chen, X. Zhu, *J. Anal. Appl. Pyrol.* 104 (2013) 514–520.
- [10] C. Li, H. Bai, G. Shi, *Chem. Soc. Rev.* 38 (2009) 2397–2409.
- [11] C.A. Kelley, B.T. Hamner, R.B. Coffin, *Environ. Sci. Technol.* 31 (1997) 2469–2472.
- [12] C.H. Christensen, J. Rass-Hansen, C.C. Marsden, E. Taarning, K. Egeblad, *ChemSusChem* 1 (2008) 283–289.
- [13] J. Ralph, G. Brunow, W. Boerjan, *Lignins. Encyclopedia of Life Science*, Wiley, Chichester, 2007.
- [14] S. Dutta, K.C.W. Wu, B. Saha, *Catal. Sci. Technol.* 4 (2014) 3785–3799.
- [15] J. Zakzeski, P.C.A. Bruijninx, A.L. Jongerius, B.M. Weckhuysen, *Chem. Rev.* 110 (2010) 3552–3599.
- [16] E.M. Anderson, R. Katahira, M. Reed, M.G. Resch, E.M. Karp, G.T. Beckham, Y. Román-Leshkov, *ACS Sustain. Chem. Eng.* 4 (2016) 6940–6950.
- [17] K.L. Deutsch, B.H. Shanks, *Appl. Catal. A* 447–448 (2012) 144–150.

- [18] X. Huang, T.I. Korányi, M.D. Boot, E.J.M. Hensen, *Green Chem.* 17 (2015) 4941–4950.
- [19] X. Huang, O.M. Morales Gonzalez, J. Zhu, T.I. Korányi, M.D. Boot, E.J.M. Hensen, *Green Chem.* 19 (2017) 175–187.
- [20] K.H. Kim, B.A. Simmons, S. Singh, *Green Chem.* 19 (2017) 215–224.
- [21] S. Van den Bosch, W. Schutyser, S.F. Koelewijn, T. Renders, C.M. Courtin, B.F. Sels, *Chem Commun.* 51 (2015) 13158–13161.
- [22] J. Zhang, J. Teo, X. Chen, H. Asakura, T. Tanaka, K. Teramura, N. Yan, *ACS Catal.* 4 (2014) 1574–1583.
- [23] J.M. Nichols, L.M. Bishop, R.G. Bergman, J.A. Ellman, *J. Am. Chem. Soc.* 132 (2010) 12554–12555.
- [24] T. Nimmanwudipong, R.C. Runnebaum, D.E. Block, B.C. Gates, *Energy Fuels* 25 (2011) 3417–3427.
- [25] T. Nimmanwudipong, C. Aydin, J. Lu, R.C. Runnebaum, K.C. Brodwater, N.D. Browning, D.E. Block, B.C. Gates, *Catal. Lett.* 142 (2012) 1190–1196.
- [26] X. Li, T. Guo, Q. Xia, X. Liu, Y. Wang, *ACS Sustain. Chem. Eng.* 6 (2018) 4390–4399.
- [27] Q. Song, J. Cai, J. Zhang, W. Yu, F. Wang, J. Xu, *Chin. J. Catal.* 34 (2013) 651–658.
- [28] C. Zhang, J. Lu, X. Zhang, K. MacArthur, M. Heggen, H. Li, F. Wang, *Green Chem.* 18 (2016) 6545–6555.
- [29] A. Wang, H. Song, *Bioresour. Technol.* 268 (2018) 505–513.
- [30] A. Wang, D. Austin, H. Song, *Fuel* 246 (2019) 443–453.
- [31] H. Liu, E. Iglesia, *J. Phys. Chem. B* 109 (2005) 2155–2163.
- [32] S. Iqbal, S.A. Kondrat, D.R. Jones, D.C. Schoenmakers, J.K. Edwards, L. Lu, B.R. Yeo, P.P. Wells, E.K. Gibson, D.J. Morgan, *ACS Catal.* 5 (2015) 5047–5059.
- [33] N. Duong, Q. Tan, D.E. Resasco, *C.R. Chim.* 21 (2018) 155–163.
- [34] M.J. Gilkey, P. Panagiotopoulou, A.V. Mironenko, G.R. Jenness, D.G. Vlachos, B. Xu, *ACS Catal.* 5 (2015) 3988–3994.
- [35] A.V. Mironenko, D.G. Vlachos, *JACS* 138 (2016) 8104–8113.
- [36] M. Verziu, A. Tirsoaga, B. Cojocar, C. Bucur, B. Tudora, A. Richel, M. Aguedo, A. Samikannu, J.P. Mikkola, *Mol. Catal.* 450 (2018) 65–76.
- [37] H. Li, G. Song, *ACS Catal.* (2019) 4054–4064.
- [38] S. Aouad, E. Saab, E. Abi-Aad, A. Aboukais, *Kinet. Catal.* 48 (2007) 835–840.
- [39] W. Li, H. Liu, E. Iglesia, *J. Phys. Chem. B* 110 (2006) 23337–23342.
- [40] S. Hosokawa, H. Kanai, K. Utani, Y.-i. Taniguchi, Y. Saito, S. Imamura, *Appl. Catal. B* 45 (2003) 181–187.
- [41] P. Betancourt, A. Rives, R. Hubaut, C.E. Scott, J. Goldwasser, *Appl. Catal. A* 170 (1998) 307–314.
- [42] G.R. Tauszik, G. Leofanti, S. Galvagno, *J. Mol. Catal.* 25 (1984) 357–366.
- [43] J. Zheng, S. Meyer, K. Köhler, *Appl. Catal. A* 505 (2015) 44–51.
- [44] T.L. Stuchinskaya, M. Musawir, E.F. Kozhevnikova, I.V. Kozhevnikov, *J. Catal.* 231 (2005) 41–47.
- [45] C. Wang, C. Tian, Y. Guo, Z. Zhang, W. Hua, W. Zhan, Y. Guo, L. Wang, G. Lu, J. Hazard. Mater. 342 (2018) 290–296.
- [46] X. Huo, D.J. Van Hooymissen, J. Liu, S. Vyas, T.J. Strathmann, *Appl. Catal. B Environ.* 211 (2017) 188–198.
- [47] Ž. Petrović, M. Ristić, M. Marciuš, B. Sepiol, H. Peterlik, M. Ivanda, S. Musić, *Ceram. Int.* 41 (2015) 7811–7815.
- [48] M. Hiratani, Y. Matsui, K. Imagawa, S. Kimura, *Thin Solid Films* 366 (2000) 102–106.
- [49] M. Wang, W. Weng, H. Zheng, X. Yi, C. Huang, H. Wan, *J. Nat. Gas Chem.* 18 (2009) 300–305.
- [50] J. Chen, J. Li, Y. Zhao, Y. Zhang, J. Hong, *J. Nat. Gas Chem.* 21 (2012) 673–679.
- [51] J. Kang, S. Zhang, Q. Zhang, Y. Wang, *Angew. Chem. Int. Ed.* 48 (2009) 2565–2568.
- [52] M. Verziu, A. Tirsoaga, B. Cojocar, C. Bucur, B. Tudora, A. Richel, M. Aguedo, A. Samikannu, J.P. Mikkola, *Mol. Catal.* 450 (2018) 65–76.
- [53] L. Dong, L.-L. Yin, Q. Xia, X. Liu, X.-Q. Gong, Y. Wang, *Catal. Sci. Technol.* 8 (2018) 735–745.
- [54] S. Ren, F. Huang, J. Zheng, S. Chen, H. Zhang, *Int. J. Hydrogen Energy* 42 (2017) 5105–5113.
- [55] B.D. Cullity, S.R. Stock, *Elements of X-Ray Diffraction*, 3rd ed., Pearson Education Limited, Harlow, 2001.
- [56] L.-P. Xiao, S. Wang, H. Li, Z. Li, Z.-J. Shi, L. Xiao, R.-C. Sun, Y. Fang, G. Song, *ACS Catal.* 7 (2017) 7535–7542.
- [57] C. Zhang, J. Lu, X. Zhang, K. MacArthur, M. Heggen, H. Li, F. Wang, *Green Chem.* 18 (2016) 6545–6555.
- [58] R. Barton, M. Carrier, C. Segura, J. Fierro, S. Park, H. Lamb, N. Escalona, S. Peretti, *Appl. Catal. A* 562 (2018) 294–309.
- [59] Y. Cao, R. Ma, N. Wang, M.-Y. Wang, X.-D. Li, L.-N. He, *J. CO2 Util.* 24 (2018) 328–333.
- [60] X. Zhou, J. Mitra, T.B. Rauchfuss, *ChemSusChem* 7 (2014) 1623–1626.
- [61] S. Wendt, M. Knapp, H. Over, *JACS* 126 (2004) 1537–1541.
- [62] A. Bjelić, M. Grilc, M. Huš, B. Likozar, *Chem. Eng. J.* 359 (2019) 305–320.
- [63] J.K. Nørskov, J. Rossmeisl, A. Logadottir, L. Lindqvist, J.R. Kitchin, T. Bligaard, H. Jonsson, *J. Phys. Chem. B* 108 (2004) 17886–17892.
- [64] D. Liu, Y.M. López-De Jesús, J.R. Monnier, C.T. Williams, *J. Catal.* 269 (2010) 376–387.
- [65] J. Jae, W. Zheng, A.M. Karim, W. Guo, R.F. Lobo, D.G. Vlachos, *ChemCatChem* 6 (2014) 848–856.
- [66] Y. Zhang, J. Yu, H. Niu, H. Liu, *J. Colloid Interface Sci.* 313 (2007) 503–510.
- [67] C. Cheng, D. Shen, S. Gu, K.H. Luo, *Catal. Sci. Technol.* 8 (2018) 6275–6296.
- [68] J. Garcia, H. Gomes, P. Serp, P. Kalck, J. Figueiredo, J. Faria, *Carbon* 44 (2006) 2384–2391.
- [69] F. Michalek, D. Mäde, J. Rühe, W. Bannwarth, *Eur. J. Org. Chem.* 2006 (2006) 577–581.
- [70] M. Besson, P. Gallezot, *Catal. Today* 81 (2003) 547–559.
- [71] N. Grosjean, C. Descorme, M. Besson, *Appl. Catal. B* 97 (2010) 276–283.